Supplemental material

Bagonis et al., https://doi.org/10.1083/jcb.201711023

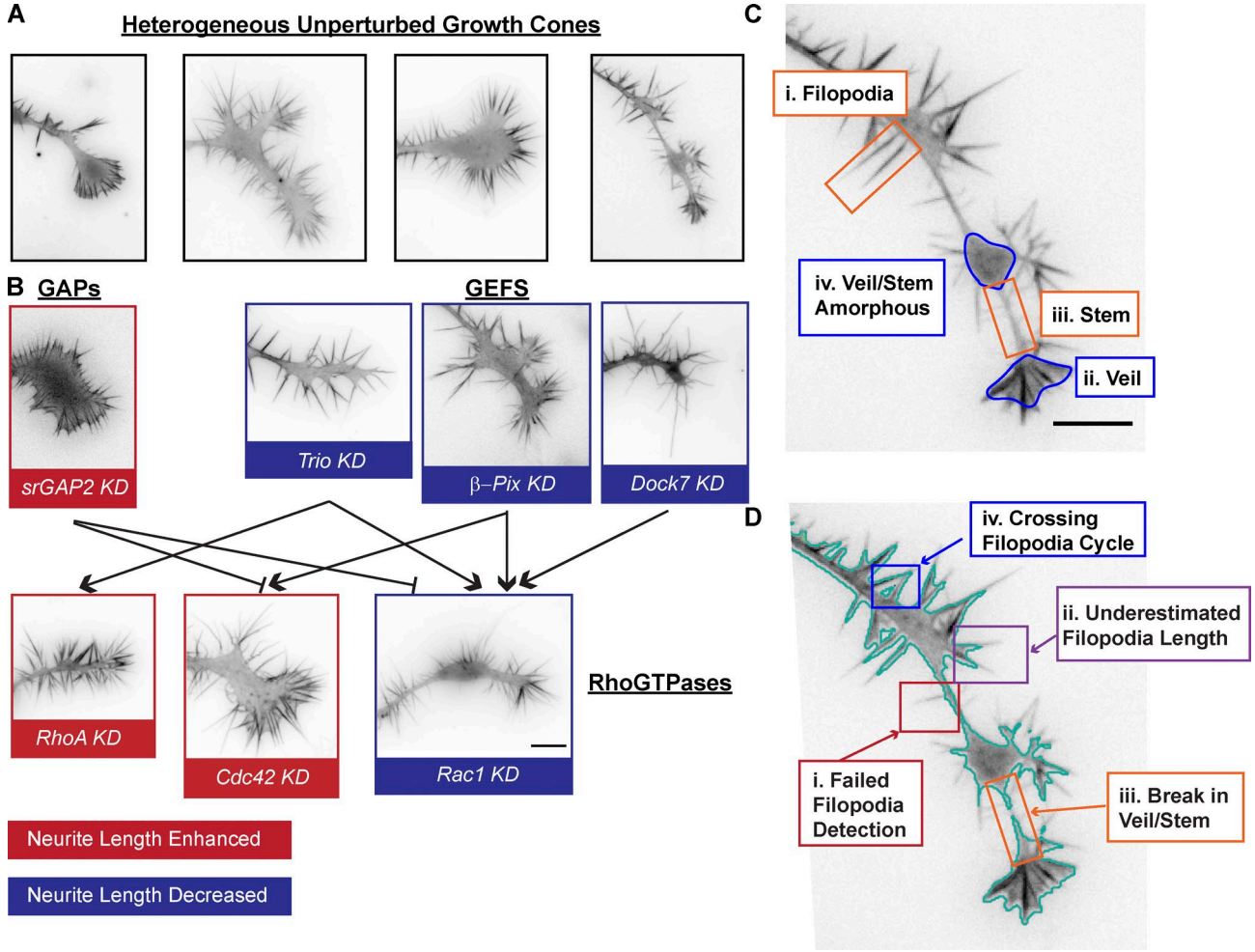

Figure S1. **Representative images of differentiated N1E-115 GCs expressing LifeAct GFP plated on laminin. (A and B)** GCs in both unperturbed (A) and perturbed (B) conditions are morphologically diverse. KD by RNAi of select nodes in the Rho GTPase signaling pathway are indicated. Perturbation conditions are color-coded by their neurite length phenotype identified in previous studies (see the GC scale morphodynamic phenotypes section for references). **(C)** Complex GC geometries arise from the superposition of filopodia actin bundles (i), the lamellipodia/veil actin network (ii), the consolidated stem (iii), and the deconsolidated veil/stem regions (iv). Color of boxes: portions of the neurite generally well-detected (orange) and ill-detected (blue) using a ridge detector. **(D)** Global thresholding–based methods for segmentation (green lines) are frequently insufficient for automated quantification of GC morphology. Illustration of common problems (i–iv). Fluorescence images are shown in inverted black/white contrast. Bar, 10 µm.

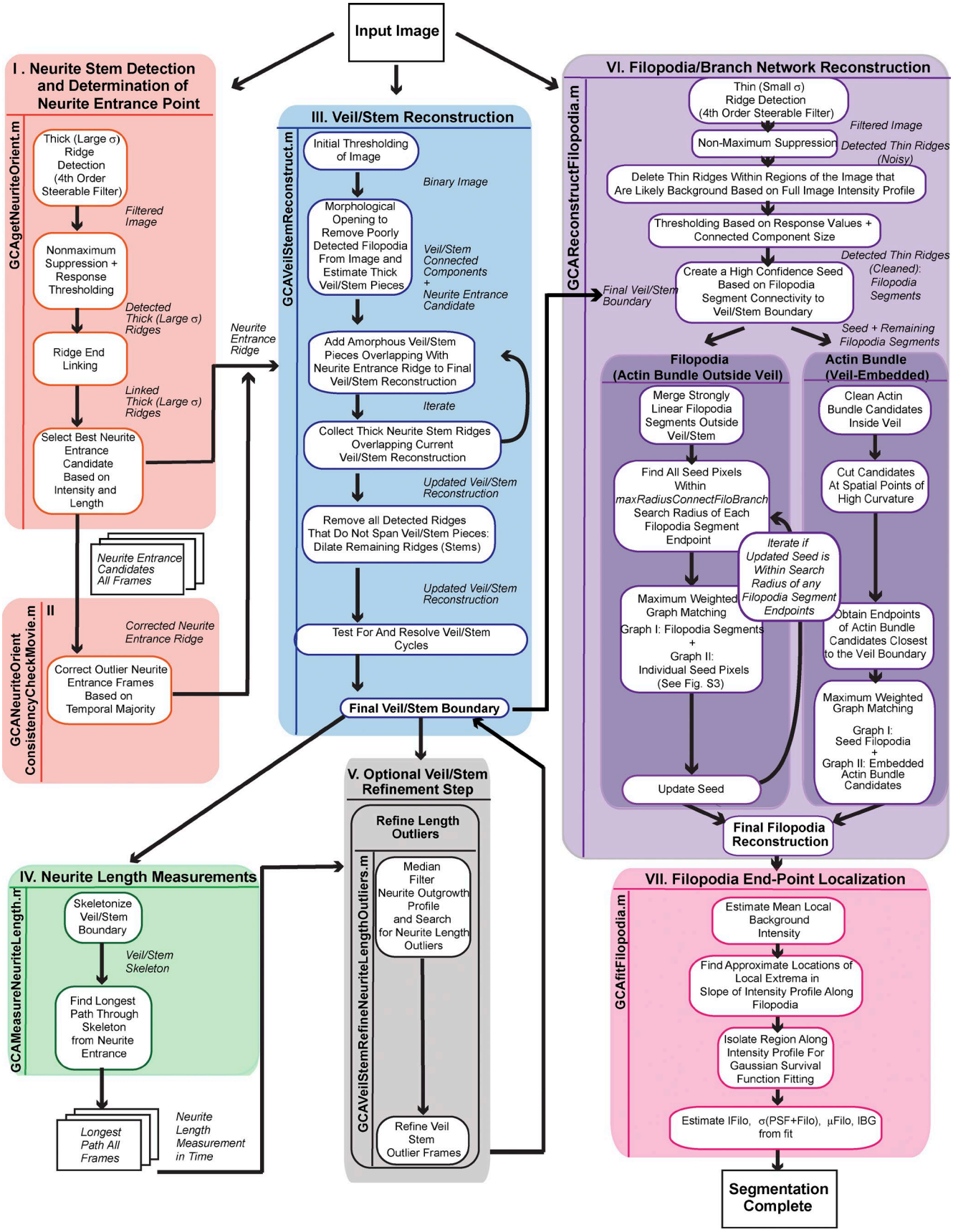

Figure S2. **Flow chart of the GCA algorithm for segmentation.** Colored blocks: different steps in the GCA segmentation. Function names corresponding to each module are located along the side of each block. IFilo: amplitude of the filament intensity above the mean background IBG (as shown in Fig. 1 A, ix).

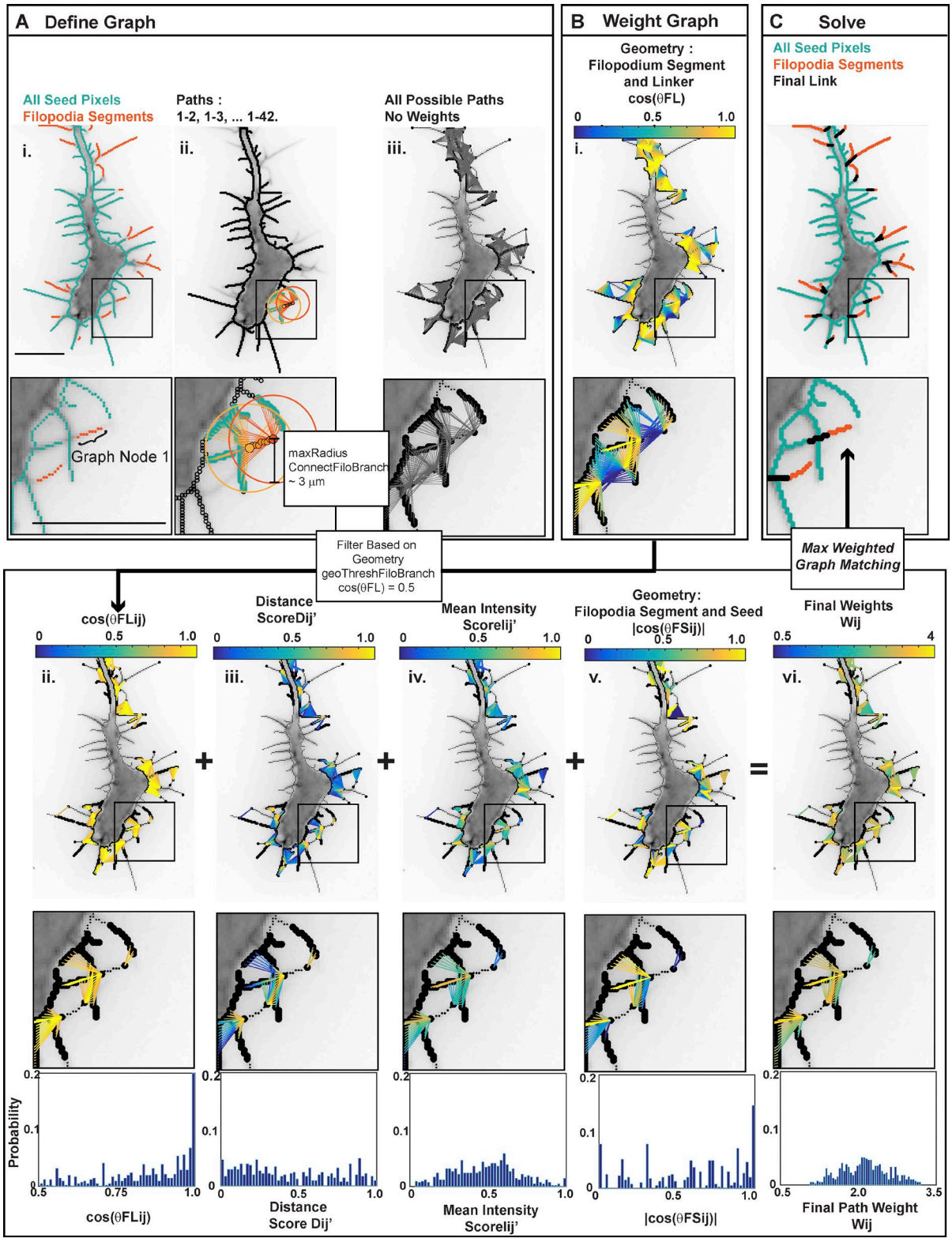

Figure S3. **Formulation of filopodia/branch reconstruction as a graph matching problem. (A)** Detected components of the GC can be defined in terms of a bipartite graph. (i) Each filopodium segment (orange) and each seed pixel (green) are potential graph nodes. (ii) Example of graph edges (orange rays) for a single filopodium segment. Only seed pixels (green highlights) within a user-defined radius (orange circles) of each filopodium segment's two endpoints are considered. (iii) All unweighted graph edges (gray rays). **(B)** Definition of graph weights. Graph edges colored by geometric continuity of the filopodium segment and the linker before (i) and after (ii) filtering of edges based on this geometry. Edges colored by (iii) Euclidean distance, (iv) mean intensity, and (v) the local orientation of the seed and the filopodia segment. Values (ii–v) are combined linearly for each edge to obtain final weights in vi. Middle: Zoom of boxed region in the upper panel. Bottom: Histograms corresponding to the distribution of all individual edge scores (ii–v), contributing to the final edge weights (vi). **(C)** Resolved graph. The maximum weighted graph matching solution. Black lines: selected edges.

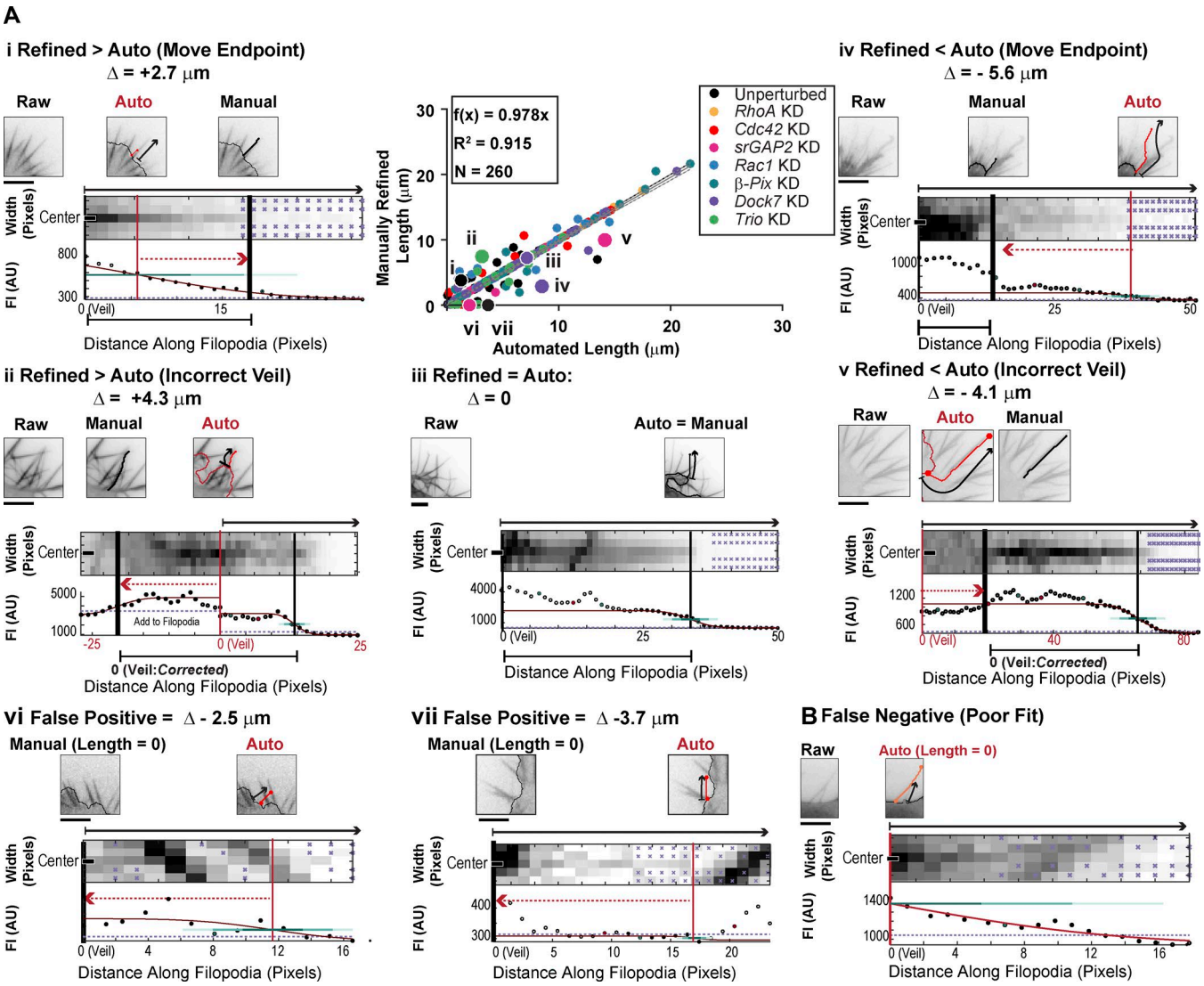

Figure S4. **Details corresponding to the manual documentation of filopodia length errors. (A)** Visualization of manual refinements based on automated GCA filopodia linescans. (i and ii) underestimation or (iv and v) overestimation, of the filopodia length by GCA due to incorrect endpoint (i and iv) or veil localization (ii and v). (iii) Accurate filopodium length confirmed visually. (vi and vii) Intensity decays of example false positives. Extension of Fig. 2 E. N, number of randomly selected filopodia length segmentations for validation. Linescans along filopodia as described in Materials and methods. **(B)** False-negative filopodium due to poor localization of fit region. Individual top panel zooms: filopodia overlays before (red) and after manual refinement (black). Black arrows: direction of the local filopodia intensity linescans (middle panels) as described in Materials and methods. Red lines: respective endpoint or veil localization error. Red arrows: manual refinement performed. Black lines with crosshairs: filopodia length after manual refinement. Bar, 5 μm.

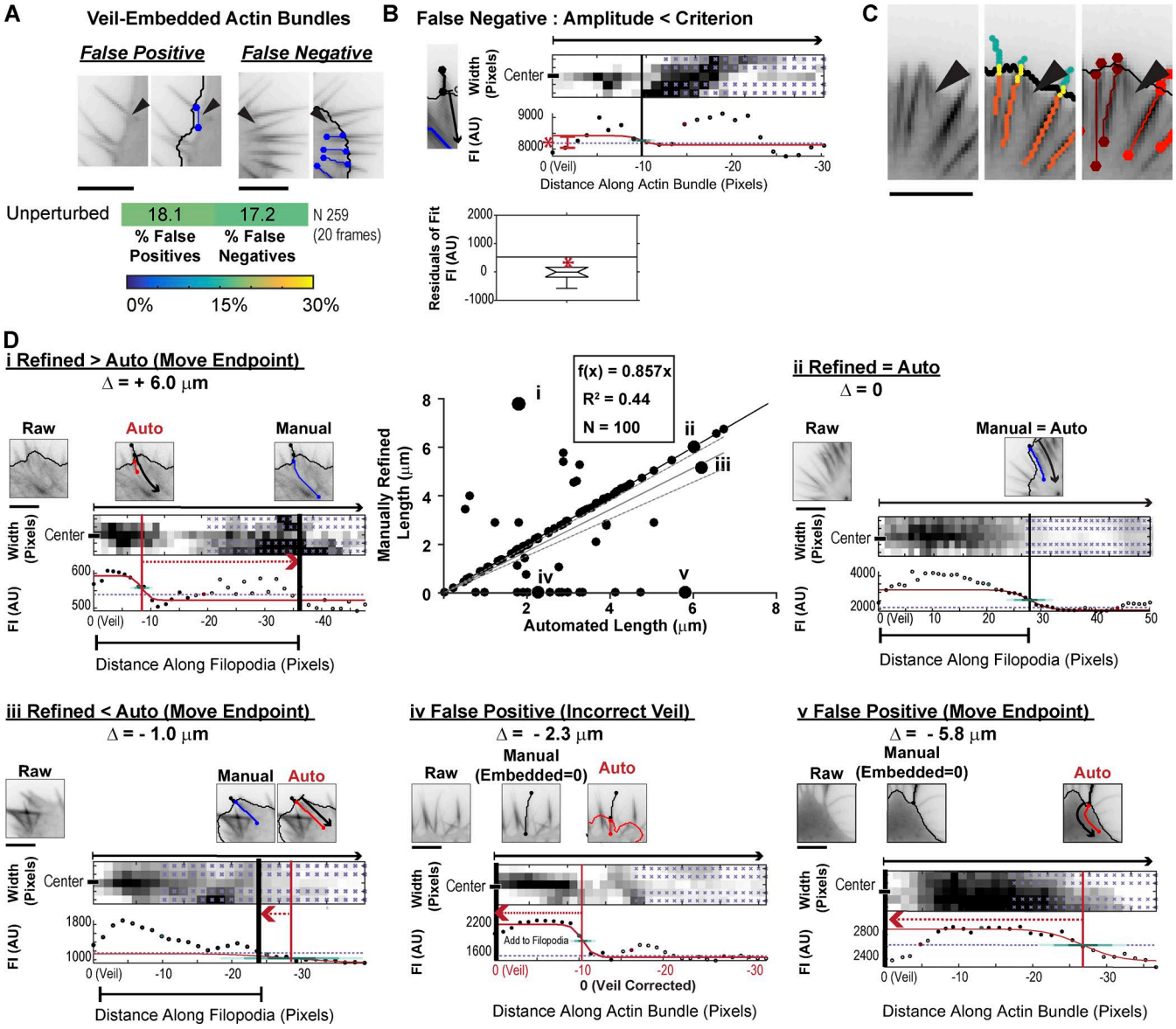

Figure S5. **Quantification of GCA error corresponding to embedded actin bundles. (A)** Quantification of GCA detection error for actin embedded actin bundles. Top: Overlays of example detection errors. Black arrow heads highlight the filopodia error. Bottom: Heat map of error rates calculated for unperturbed condition for randomly selected frames of the N1E-115 dataset (one per movie). N, number of filopodia manually analyzed. **(B)** False-negative actin bundle due to final filter on the residuals of the fit. Top: Line scans along actin bundle: see Materials and methods. Filter was set to include only embedded actin structures with amplitudes (red star) above the 95th percentile of the residuals (black line). **(C)** GCA is not designed to detect fully embedded actin structures lacking an extra-veil component. Left: Raw image. Center: One-to-one geometric matching of the embedded actin bundle with its extra-veil counterpart. Cyan, extra-veil filopodia detections; orange, embedded actin bundle matches; yellow, links. Right: Final GCA segmentation. Arrowhead: A precursor actin bundle that cannot be detected. **(D)** Automated GCA actin bundle lengths to actin bundle lengths after manual check/refinement. Black line: perfect correlation. Gray solid line, linear fit to the data; gray dotted lines, CI of the fit; N, number of filopodia. Underestimation (i), accurate filopodium length (ii), overestimation (iii), and false positives due to incorrect veil (iv) or endpoint (v) localization. Individual top panel zooms: Embedded actin bundle overlays before (red) and after manual refinement (blue). Black: extra veil filopodia detection. Bar, 5 μm.

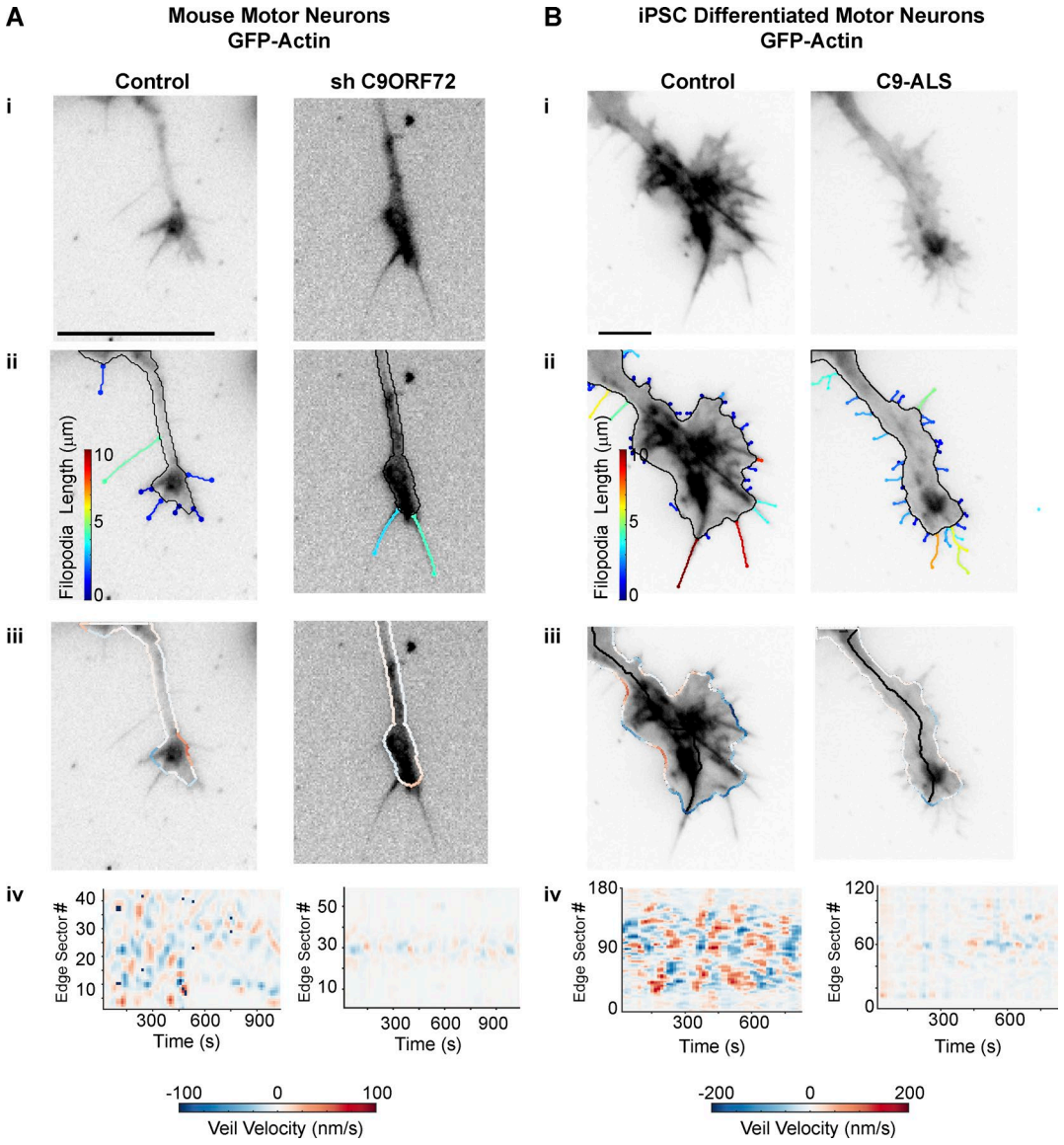

Figure S6. **GCA segmentation and veil velocity analysis applied to primary mouse and differentiated induced pluripotent stem cell (iPSC) motor neurons. (A and B)** GCA segmentation overlays (ii), veil velocity overlays (iii), and comparative veil velocity heat maps (iv) for raw images in i. (A) Mouse motor neurons expressing GFP-actin from a control (left) and sh C9ORF72 (right). (B) Differentiated iPSC motor neurons expressing GFP-actin from a control (left) and C9 amyotrophic lateral sclerosis (ALS) patient (right). Previously published raw images (Sivadasan et al., 2016) provided courtesy of the Sendtner laboratory at University of Würzburg. See Video 8. Bar, 10 µm.

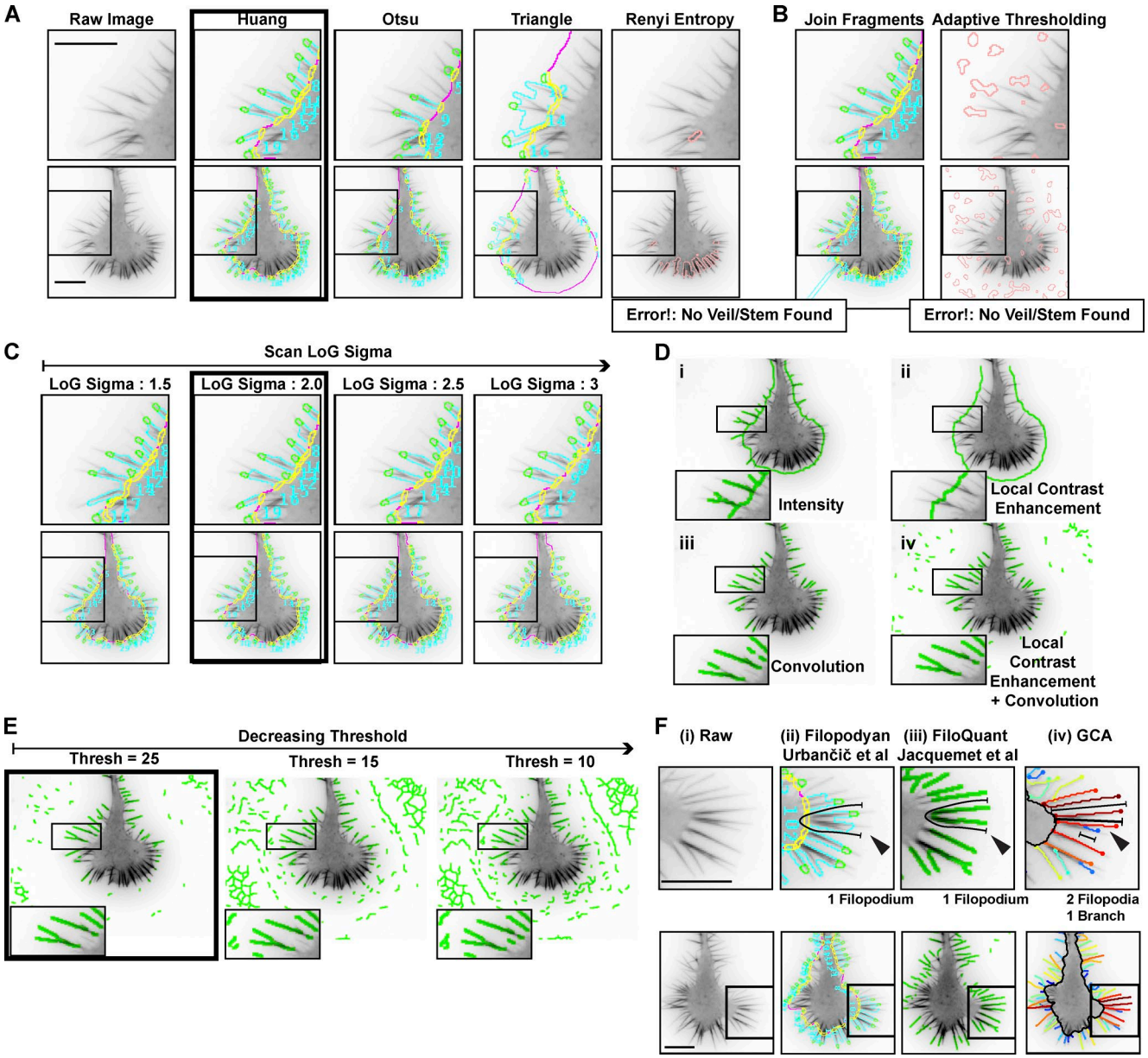

Figure S7. **Segmentation parameter scanning using previously published software. (A–C)** Segmentation parameter scans using the Filopodyan (Urbančič et al., 2017) software package (A). Scan of different global thresholding methods. (B) Scan of advanced settings. (C) Scan of LoG sigma values. Boxes: Segmentation parameters used for Fig. 4, A and B, ii. **(D and E)** Segmentation parameter scans using FiloQuant (Jacquemet et al., 2017) software package. (D) Scan of different detection methods in FiloQuant, (i) Intensity, (ii) Local Contrast Enhancement, (iii) Convolution, or (iv) Convolution + Local Contrast Enhancement. Filopodia Threshold = 25. No filopodia repair. (E) Scan of decreasing thresholds for segmentation performed with Convolution + Local Contrast Enhancement + Filopodia Repair. Boxes: segmentation parameters used for Fig. 4, A and B, iii. Canonical unperturbed N1E-115 GC labeled with GFP LifeAct. Same image as shown in Fig. 2 (A and C) and Fig. 4 A. See Materials and methods. **(F)** Segmentation overlays as generated using Filopodyan (Urbančič et al., 2017; ii), FiloQuant (Jacquemet et al., 2017; iii), and the current algorithm, GCA (iv) for the raw image shown in i using segmentation parameters optimized for an earlier frame image (A–E) of the same movie. Visualization overlays as available in each package and Fig. 4. Bar, 10 µm.

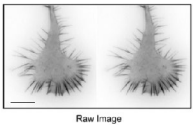

Video 1. **Visualization of GCA algorithmic steps for a canonical N1E-115 GC.** Different steps in the algorithm are shown for a single frame. Corresponds to Fig. 1 A. Bar, 10 µm.

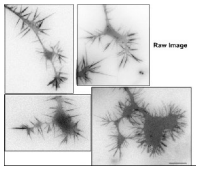

Video 2. **Visualization of GCA veil/stem reconstruction steps for four noncanonical N1E-115 GCs.** Different steps in the algorithm are shown for a single frame. Automatic algorithmic deviations for select reconstruction problems are emphasized. Visualization ends after veil/stem reconstruction is complete. Corresponds to Fig. 1 B. Bar, 10 µm.

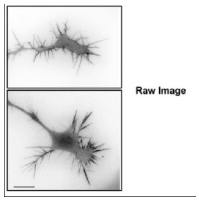

Video 3. **Visualization of GCA filopodia/branch reconstruction steps for two noncanonical N1E-115 GCs.** Different steps in the algorithm are shown for a single frame. Visualization starts after veil/stem reconstruction is complete. Algorithmic handling of actin bundle crossings (top) and branches (bottom) are emphasized. Corresponds to Fig. 1 D. Bar, 10 µm.

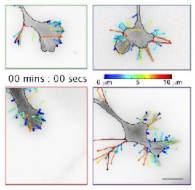

Video 4. **GCA overlays of unperturbed N1E-115 GCs, expressing LifeAct GFP, plated on laminin.** Images were acquired at 5-s time intervals for 10 min. Only the first 5 min of the original movie is shown to comply with video file size restrictions. Corresponds to Fig. 2 and Fig. 6 E. First half of the movie: actin bundle overlays (colored by length). Second half of the movie: veil/stem overlays (colored by local veil velocity) and neurite length overlays (black line). Visualized at 10 frames per second (fps). Bar, 10 µm.

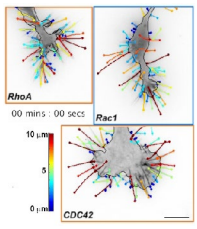

Video 5. **GCA overlays of Rac1-, Cdc42-, or RhoA siRNA–treated N1E-115 GCs, expressing LifeAct GFP, plated on laminin.** Images were acquired at 5-s time intervals for 10 min. Only the first 5 min of the original movie is shown to comply with video file size restrictions. Corresponds to Fig. 2 and Fig. 7. First half of the movie: actin bundle overlays (colored by length). Second half of the movie: veil/stem overlays (colored by local veil velocity) and neurite length overlays (black line). Visualized at 10 fps. Bar, 10 µm.

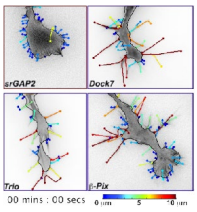

Video 6. **GCA overlays of β-pix–, Dock7-, Trio (Rac1GEFs)- or srGAP2 (Rac1 GAP) siRNA–treated N1E-115 GCs, expressing LifeAct GFP, plated on laminin.** Images were acquired at 5-s time intervals for 10 min. Only the first 5 min of the original movie is shown to comply with video file size restrictions. Corresponds to Fig. 2 and Fig. 7. First half of the movie: actin bundle overlays (colored by length). Second half of the movie: veil/stem overlays (colored by local veil velocity) and neurite length overlays (black line). Visualized at 10 fps. Bar, 10 µm.

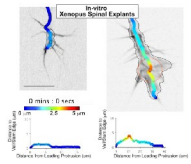

Video 7. **GCA overlays (veil/stem thickness profiles and filopodia overlays colored by length): GCs of different size, type, and fluorescent label, imaged in vitro, ex vivo, and in vivo.** Corresponds to Fig. 3, A–D. See Fig. 3 legend for references. Visualized at 10 fps. Bar, 10 µm.

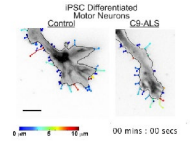

Video 8. **GCA overlays (filopodia colored by length and veil/stem colored by local veil velocity) corresponding to differentiated iPSC motor neurons (control versus C9-ALS patient) and primary mouse motor neurons (control versus sh C9ORF72).** All express GFP-actin. Images were acquired at 15-s time intervals as described in (Sivadasan et al., 2016). Movies visualized for 13 (iPSC) and 5 (primary neurons) minutes. Corresponds to Fig. S6. Visualized at 10 fps. Bar, 10 µm.

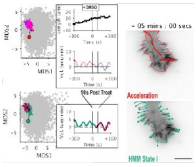

Video 9. **DMSO-treated N1E-115 GC, expressing GFP LifeAct, plated on laminin: Comparison of neurite outgrowth and HMM morphology state classifications.** Dynamic visualization of time series plots in Fig. 8 E, left, and Fig. 9 A, left, where the data point corresponding to the current image frame is highlighted. Images were acquired at 5-s time intervals for 10 min. Time of acute treatment: 5 min. Veil/stem and neurite length overlays (top, right) colored by neurite outgrowth state classification of current frame. Full segmentation overlays including filopodia (bottom, right) colored by HMM morphology state classification of current frame. Video slowed to 1 fps to emphasize the addition of the respective acute treatment and any detected HMM morphology state transitions within the 90-s post-treatment window (arrows). The remainder of the video is visualized at 10 fps. Bar, 10 µm.

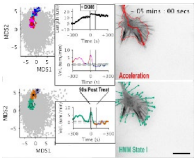

Video 10. **25 µM CK666-treated N1E-115 GC, expressing GFP LifeAct, on laminin: Comparison of neurite outgrowth and HMM morphology state classifications.** Dynamic visualization of time series plots in Fig. 8 E, right, and Fig. 9 A, right, where the data point corresponding to the current image frame is highlighted. Images were acquired at 5-s time intervals for 10 min. Time of acute treatment: 5 min. Veil/stem and neurite length overlays (top, right) colored by neurite outgrowth state classification of current frame. Full segmentation overlays including filopodia (bottom, right) colored by HMM morphology state classification of current frame. Video is slowed to 1 fps to emphasize the addition of the respective acute treatment and any detected HMM morphology state transitions within the 90-s post-treatment window (arrows). The remainder of the video is visualized at 10 fps. Bar, 10 µm.

Provided online are two tables in Excel. Table S1 lists GCA segmentation parameters, default settings, and recommendations. Table S2 provides the siRNA sequences used in this study.

References

Jacquemet, G., I. Paatero, A.F. Carisey, A. Padzik, J.S. Orange, H. Hamidi, and J. Ivaska. 2017. FiloQuant reveals increased filopodia density during breast cancer progression. *J. Cell Biol.* 216:3387–3403 http://dx.doi.org/http://dx.doi.org/10.1083/jcb.201704045. https://doi.org/10.1083/jcb.201704045

Sivadasan, R., D. Hornburg, C. Drepper, N. Frank, S. Jablonka, A. Hansel, X. Lojewski, J. Sterneckert, A. Hermann, P.J. Shaw, et al. 2016. C9ORF72 interaction with cofilin modulates actin dynamics in motor neurons. *Nat. Neurosci.* 19:1610–1618. https://doi.org/10.1038/nn.4407

Urbančič, V., R. Butler, B. Richier, M. Peter, J. Mason, F.J. Livesey, C.E. Holt, and J.L. Gallop. 2017. Filopodyan: An open-source pipeline for the analysis of filopodia. *J. Cell Biol.* 216:3405–3422 http://dx.doi.org/http://dx.doi.org/10.1083/jcb.201705113. https://doi.org/10.1083/jcb.201705113